Available online at www.sciencedirect.com
SCIENCE DIRECT®
Journal of Chromatography A, 1064 (2005) 227–237
JOURNAL OF CHROMATOGRAPHY A
www.elsevier.com/locate/chroma

Analytical study of Joule heating effects on electrokinetic transportation in capillary electrophoresis

Xiangchun Xuan, Dongqing Li*

Department of Mechanical and Industrial Engineering, University of Toronto, 5 King's College Road, Toronto, Ont., Canada M5S 3G8

Received 1 September 2004; received in revised form 28 November 2004; accepted 10 December 2004
Available online 7 January 2005

Abstract

Electric fields are often used to transport fluids (by electroosmosis) and separate charged samples (by electrophoresis) in microfluidic devices. However, there exists inevitable Joule heating when electric currents are passing through electrolyte solutions. Joule heating not only increases the fluid temperature, but also produces temperature gradients in cross-stream and axial directions. These temperature effects make fluid properties non-uniform, and hence alter the applied electric potential field and the flow field. The mass species transport is also influenced. In this paper we develop an analytical model to study Joule heating effects on the transport of heat, electricity, momentum and mass species in capillary-based electrophoresis. Close-form formulae are derived for the temperature, applied electrical potential, velocity, and pressure fields at steady state, and the transient concentration field as well. Also available are the compact formulae for the electric current and the volume flow rate through the capillary. It is shown that, due to the thermal end effect, sharp temperature drops appear close to capillary ends, where sharp rises of electric field are required to meet the current continuity. In order to satisfy the mass continuity, pressure gradients have to be induced along the capillary. The resultant curved fluid velocity profile and the increase of molecular diffusion both contribute to the dispersion of samples. However, Joule heating effects enhance the sample transport velocity, reducing the analysis time in capillary electrophoretic separations.

Keywords: Joule heating; Electrokinetic transportation; Capillary electrophoresis

1. Introduction

Microfluidic and lab-on-a-chip devices have attracted increasing interest over the last decade due to their advantages over macroscopic counterparts, such as increased efficiency and throughput, and reduced analysis time and reagent consumption [1,2]. The performance of these miniaturized systems depends on the precise control of fluids and samples through the network of microchannels. Generally, an electric field is applied to induce electroosmotic flow of fluids and electrophoretic motion of chemical species in microfluidic devices. Electrophoretic separation is such an application combining these two electrokinetic flows. It exploits the difference in electrophoretic mobilities between charged chemical species in aqueous solution, whereas the electroosmotic flow of the latter could reduce the analysis time [3]. Under ideal circumstances, the electroosmotic flow profile across a capillary is flat, and all the velocity variations are restricted to the thin electrical double layer region adjacent to the capillary wall. As such, there is negligible shear-induced dispersion so that the molecular diffusion is the only limit to separation. However, in practice, many experimental factors can affect the flow patterns, which in turn reduce the separation efficiency on account of the enhanced dispersion [4–6]. In this paper we study analytically the Joule heating effects on the electrokinetic transportations in capillary-based electrophoretic separation systems.

Joule heating results from current flow through the electrolyte solution when an electric field is applied to achieve

* Corresponding author. Tel.: +1 416 978 1282; fax: +1 416 978 7753.
E-mail address: dli@mie.utoronto.ca (D. Li).

0021-9673/$ – see front matter © 2004 Elsevier B.V. All rights reserved.
doi:10.1016/j.chroma.2004.12.033

electrokinetic flows in capillary electrophoresis. This internal heat generation is taken away not only by the coolant surrounding the capillary (through either air or liquid convection and radiation as well), but also by the cold liquid inside reservoirs connecting to the two ends of the capillary (through conduction). On neglecting the thermal end effects, Joule heating has been known to cause an increase and a radial gradient in the fluid temperature [7–11]. For this case, the profile of electroosmotic velocity remains plug-like in the bulk region despite the increased magnitude due to the drop of liquid viscosity [12]. However, both electrophoretic velocity and molecular diffusion of analyte species become non-uniform over the channel cross-section. These radial non-uniformities can cause the so-called Taylor–Aris dispersion of samples [13,14]. The problem of dispersion caused by the perturbed profile of electrophoretic velocity has been examined theoretically and experimentally [15–20]. It was found that the thermally induced dispersion is small compared to that from molecular diffusion except at some extreme conditions. This phenomenon is attributed to the generally small temperature difference across the capillary lumen. Only till recently has the extra dispersion due to the radial non-uniformity of molecular diffusion been taken into consideration in Xuan and Li's analytical model [21]. More recently, Peterson et al. provided a closer look on Joule heating effects in microchip-based and capillary-based electrophoretic separation systems [22]. These authors argued that the main influence of Joule heating effects on separation efficiency is via the radial temperature profile, not the overall temperature rise in the buffer solution.

In the presence of reservoir-based thermal end effects, however, Joule heating leads to both radial and axial temperature variations in the electrolyte solution. Through a combined experimental and numerical study of the electroosmotic flow in a free-air cooled capillary, Li's group observed sharp temperature drops near the ends of the capillary and a high temperature plateau in the middle section [23,24]. Due to the temperature dependence of electric conductivity of the liquid, these axial temperature gradients make the electric field non-uniform along the channel. As a result, axial pressure gradients are induced in order to maintain the fluid continuity during the flow. This numerical prediction was confirmed by the observation of concave–convex–concave fluid velocity profiles from the inlet to the outlet of the capillary. In addition, Yang's group conducted a numerical analysis of the thermal effect on electroosmotic flow and electrokinetic mass transport in both cylindrical and slit microchannels [25,26]. They predicted a concave fluid velocity profile in the main channel with the assumption of a uniform electric field along the channel. Unfortunately, the complicated and time-consuming simulations available so far could not provide a straightforward understanding of Joule heating effects on electrokinetic transportations. Moreover, Joule heating effects on the transport of sample zone in capillary electrophoretic separations have yet to be studied.

Axial temperature gradients could also arise from the variation of heat transfer condition [27] or the variation of buffer conductivity along the capillary [28]. The latter may exist in the so-called sample pumping and stacking processes [29]. The variation of heat transfer condition along a capillary is often present in capillary electrophoresis with thermostating, where a short length of the capillary at each end must be left outside the thermostating cartridge for the sample injection and detection, respectively [18,19]. Xuan and Li [30] investigated the flow perturbation and the sample dispersion in such a thermostated capillary electrophoresis. By assuming step changes of fluid temperature in regions with different heat transfer conditions, both non-uniform electric field and non-uniform electroosmotic velocity along the capillary were found in order to meet the current and mass continuities. This modification of the plug-like pattern of fluid electroosmotic flow could cause significantly higher dispersion than that from parabolic-like electrophoretic flow profile due to radial temperature gradients. Essentially, the increased dispersion caused by axial temperature gradients is identical to that caused by the non-uniformity of zeta potential along the capillary [31–34].

In the next section, the mathematical formulation of Joule heating effects on electrokinetic transportations in capillary electrophoresis is presented. A uniform heat transfer condition is assumed along the capillary, corresponding exactly to capillary electrophoresis with free-air cooling. Analytical formulae for the perturbed temperature field, applied electric potential field and flow field are derived in order. Then, the transient concentration field of sample species is analyzed based on the well-developed Taylor–Aris dispersion theory. The inclusion of the temperature dependence of fluid properties in the formulation should make the present model applicable to most practical capillary-based electrophoretic separation systems.

2. Mathematical formulation

Consider a long cylindrical capillary of internal radius R_l (i.e., liquid domain) and length L_0. The outer radii of the glass wall and the polyimide coating (i.e., the total radius of the capillary) are R_w and R_p, respectively. Note that $L_0 \gg R_p$ is available in typical capillary electrophoresis. Owing to the axisymmetric nature, a 2D cylindrical coordinate system (r, z) is adopted with the origin at the capillary inlet and x-axis along the capillary centerline. According to previous studies, the temperature field in capillary electrophoresis approaches steady state at several seconds [17,24,35]. The sample separation process may, however, take up to tens of minutes to finish [3]. Therefore, we start with the steady state temperature and flow fields. After that, the transient development of concentration field is analyzed.

2.1. Temperature field

As mentioned above, the Joule heat generated inside the buffer solution is taken away in two ways: one is through the convective and radiant cooling from the capillary outer surface, and the other is through the conductive cooling from the capillary ends (i.e., thermal end effects). These two cooling methods are reflected in the boundary conditions of the energy equation. Neglecting the radial convective heat transport [36], the fluid temperature is solved from:

$$\frac{1}{r}\frac{\partial}{\partial r}\left(r\frac{\partial T}{\partial r}\right)+\frac{\partial^2 T}{\partial z^2}-\frac{u_z}{\alpha_l}\frac{\partial T}{\partial z}+\frac{\lambda_l E^2}{k_l}=0 \tag{1}$$

$$T(r,0)=T(r,L_0)=T_0 \tag{2}$$

$$\frac{\partial T}{\partial r}(0,z)=0 \tag{3}$$

$$\frac{\partial T}{\partial r}(R_l,z)=-\frac{h_{eq}}{k_l}[T(R_l,z)-T_0] \tag{4}$$

where E is the local electrical field strength, u_z the axial fluid velocity, α_l, k_l and λ_l the thermal diffusivity, thermal conductivity and electrical conductivity of the buffer solution, respectively. A linear model is employed to describe the temperature dependence of electrical conductivity

$$\lambda_l=\lambda_0[1+\alpha(T-T_0)] \tag{5}$$

where λ_0 is the electrical conductivity at the room temperature T_0 (298 K), and α the temperature coefficient. The equivalent heat transfer coefficient h_{eq} is given by:

$$h_{eq}=R_l^{-1}\left[\frac{1}{k_w}\ln\left(\frac{R_w}{R_l}\right)+\frac{1}{k_p}\ln\left(\frac{R_p}{R_w}\right)+\frac{1}{hR_p}\right]^{-1} \tag{6}$$

where k_w and k_p are respectively, the thermal conductivities of the capillary wall and polyimide coating, and h the surface heat transfer coefficient between the coolant and the capillary outer surface. Here we have assumed a constant thermal conductivity because the thermal conductivity of aqueous solution is much less sensitive to temperature change in comparison with the electrical conductivity. Within the range of the temperature change considered in this work, the variation in thermal conductivity is negligible.

In typical capillary electrophoresis the temperature variation over r is much smaller than that in the axial direction [21,22,30]. This indicates $T=T(z)$ only, as a good approximation. Hence, the local fluid temperature can be replaced by the cross-sectional average $\bar{T}(z)$ (at constant z). We acknowledge that this approximation may not be valid for capillary electrophoresis with thermostating [8,10]. In such cases, however, the sample dispersion induced by the temperature jump between thermostated and unthermostated regions is more pronounced than that due to thermal end effects [30]. Averaging each term in Eq. (1) over the capillary cross-section yields:

$$\frac{d^2\bar{T}}{dz^2}-\frac{\bar{u}}{\alpha_l}\frac{d\bar{T}}{dz}-\frac{2h_{eq}}{k_l R_l}(\bar{T}-T_0)+\frac{\lambda_0[1+\alpha(\bar{T}-T_0)]E^2}{k_l}=0 \tag{7}$$

where the surface temperature $T(R_l, z)$ in Eq. (4) has been approximated to $\bar{T}(z)$. The mean fluid velocity $\bar{u}$ in Eq. (7) is a constant in a uniform capillary according to the condition of mass continuity, and will be specified later in this paper. Note also that the local electric field is parallel to the capillary axis and therefore dependent only on z. The requirement of current continuity through the uniform capillary leads to

$$\lambda E=\lambda_0[1+\alpha(\bar{T}-T_0)]E=J \tag{8}$$

where J denotes the electric current density to be determined in the next section. Then, we can assume

$$\lambda_0[1+\alpha(\bar{T}-T_0)]E^2\cong J^2[1-\alpha(\bar{T}-T_0)]/\lambda_0 \tag{9}$$

for small values of $\alpha(\bar{T}-T_0)$, say <0.25. For even larger temperature rise, however, higher order terms of $\alpha(\bar{T}-T_0)$ are indispensable in Eq. (9), which will greatly complicates the derivations hereafter. By the definitions of $Z=z/R_l$ and $\Theta=(\bar{T}-T_0)/\Delta T$ and the substitution of Eq. (9), Eq. (7) is written into the following non-dimensional form

$$\frac{d^2\Theta}{dZ^2}-\frac{\bar{u}R_l}{\alpha_l}\frac{d\Theta}{dZ}-\left(\frac{2h_{eq}R_l}{k_l}+\alpha\Delta T\right)\Theta+1=0 \tag{10a}$$

$$\Delta T=\frac{J^2R_l^2}{\lambda_0 k_l} \tag{10b}$$

Noting the Dirichlet boundary conditions in Eq. (2), we can obtain

$$\Theta(Z)=\frac{1}{\beta^2}\left[1-\frac{(e^{A_1L}-1)e^{A_2(L-Z)}+(e^{A_2L}-1)e^{A_1Z}}{e^{(A_2+A_2)L}-1}\right] \tag{11a}$$

$$\beta=\sqrt{2h_{eq}R_l/k_l+\alpha\Delta T} \tag{11b}$$

$$A_1=\sqrt{\frac{1}{4}\left(\frac{\bar{u}R_l}{\alpha_l}\right)^2+\beta^2}+\frac{1}{2}\left(\frac{\bar{u}R_l}{\alpha_l}\right) \tag{11c}$$

$$A_2=\sqrt{\frac{1}{4}\left(\frac{\bar{u}R_l}{\alpha_l}\right)^2+\beta^2}-\frac{1}{2}\left(\frac{\bar{u}R_l}{\alpha_l}\right) \tag{11d}$$

where $L=L_0/R_l$ indicates the non-dimensional length of the capillary, and $L\gg 1$ is implied. Note that $h_{eq}R_l/k_l$ in Eq. (11b) and $\bar{u}R_l/\alpha_l$ in Eqs. (11c) and (11d) represent, respectively, the so-called Biot number and Peclet number. Ordinarily, $(\bar{u}R_l/\alpha_l)=O(\beta)$ and $\beta=O(1)$. The fluid temperature is asymmetric about the middle section of the capillary since $A_1\neq A_2$ due to the flow effect. Noting $\exp(-x)\to 0$ unless x is small, the fully developed fluid temperature is approximated to $1/\beta^2$. This temperature is dependent on the electric

current density J that will be determined in the next section. On assuming a positive $\bar{u}$ in Eq. (11a–d), the thermal entrance length that corresponds to the temperature reaching 99% of the fully developed temperature is estimated as 4.605 R_l/A_2 (see Appendix A for the computation). Similarly, the length of thermal exit region, where temperatures undergo rapid variations to adjust to the fluid temperature at the outlet reservoir, is given by 4.605 R_l/A_1. Since $A_1 > A_2$ at a positive $\bar{u}$ (see Eqs. (11c) and (11d)), the axial temperature profile is actually inclined to the direction of fluid flow, i.e., the downstream.

2.2. Applied electric potential field

In the above derivation of temperature field, the electric current density J in Eq. (8) remains unknown. We can determine J from the current continuity since the axial temperature distribution is now available. Rearranging Eq. (8) leads to:

$$E = \frac{-\mathrm{d}\phi}{\mathrm{d}z} \cong \frac{J\left[1-\alpha(\bar{T}-T_0)\right]}{\lambda_0} \tag{12}$$

where ϕ is the applied electric potential. Eq. (12) can be rewritten as

$$\frac{\mathrm{d}\Phi}{\mathrm{d}Z} = \frac{-JR_l\,(1-\alpha\Delta T\Theta)}{\lambda_0\phi_0} \tag{13}$$

where $\Phi = \phi/\phi_0$ and $\phi_0 = E_0L_0$ with E_0 being the electric field strength externally applied to the capillary. Integrating Eq. (13) along the channel with $\Phi(0) = 1$ and $\Phi(L) = 0$ (i.e., the capillary outlet is grounded) gives rise to

$$\frac{\lambda_0\phi_0}{JR_l} = L - \frac{\alpha\Delta T}{\beta^2}\left[L - \frac{(\mathrm{e}^{A_1L}-1)(\mathrm{e}^{A_2L}-1)(1/A_1+1/A_2)}{\mathrm{e}^{(A_2+A_2)L}-1}\right] \tag{14a}$$

$$\frac{\lambda_0\phi_0}{JR_l} \cong L\left(1-\frac{\alpha\Delta T}{\beta^2}\right) \tag{14b}$$

where $L \gg 1$ and hence $\mathrm{e}^{A_1L} = O(\mathrm{e}^{A_2L}) >> 1$ are necessary in making the approximation in Eq. (14b). After recovering ΔT and β in Eq. (14b), we can get a compact formula for the electric current density

$$J = \frac{h_{\mathrm{eq}}}{\alpha R_l E_0}\left(1-\sqrt{1-2\lambda_0 E_0\frac{\alpha R_l E_0}{h_{\mathrm{eq}}}}\right) \tag{15}$$

The terms within the square root imposes a limit to the applied electric field E_0, beyond which the solution to J is unavailable. This limit is attributed to the linear approximation made in Eqs. (9) and (12) which differs from the limitation due to the so-called thermal run-away [11,21,30]. One can also see that J in Eq. (15) is independent of the capillary length, so is the fully developed fluid temperature $1/\beta^2$ (nondimensional) obtained earlier (see Eqs. (10b) and (11b)). As the temperature coefficient $\alpha \to 0$, J approaches λ_0E_0 representing the electric current density without considering either the temperature dependence of electrical conductivity ($\alpha = 0$) or the Joule heating effects. At this stage, the electric current density is available from Eq. (15). However, there is still one unknown parameter in the temperature field (see Eq. (11a–d)) and thus the electric field (see Eq. (12)), i.e., the mean fluid velocity $\bar{u}$. We will present its formula in the next section.

2.3. Flow field

Similar to the treatment of thermal conductivity in energy Eq. (1), we assume a constant density of the buffer solution in the analysis of flow field. Since we are only concerned with the steady-state flow field, the transient terms in Navier–Stokes equations drop off. The inertial terms are also neglected because fluid flows in capillary electrophoresis are generally limited to small Reynolds numbers. Noting that the length scale in the axial direction is much larger than that in the radial direction, the axial velocity component u_z has to be much higher than the radial component u_r in order to satisfy the continuity equation. In other words, the present fluid flow is nearly unidirectional [37]. After comparing the orders of magnitude, Navier–Stokes equations and the continuity equation give rise to:

$$\frac{1}{r}\frac{\partial}{\partial r}\left(r\frac{\partial u_z}{\partial r}\right) = \frac{1}{\mu}\frac{\partial p}{\partial z} \tag{16}$$

$$\frac{\partial p}{\partial r} = 0 \tag{17}$$

$$\frac{1}{r}\frac{\partial}{\partial r}(ru_r) + \frac{\partial u_z}{\partial z} = 0 \tag{18}$$

$$u_z(R_l, z) = u_{\mathrm{eo}} \tag{19}$$

$$\partial u_z/\partial r(0, z) = 0 \tag{20}$$

$$u_r(0, z) = u_r(1, z) = 0 \tag{21}$$

where p is the hydrodynamic pressure, and the slip velocity u_{eo} in Eq. (19) is calculated from the Helmholtz–Smoluchowshi formula [38]:

$$u_{\mathrm{eo}} = \frac{-\varepsilon\zeta E}{\mu} \tag{22}$$

where ε and μ are the dielectric constant and the dynamic viscosity of the buffer solution, respectively, and ζ the zeta potential. These properties are usually dependent on the fluid temperature, and thus vary along the capillary. This indicates $u_{\mathrm{eo}} = u_{\mathrm{eo}}(z)$. The above slip boundary condition applies to electroosmotic flow with an infinitely thin electric double layer, which is an excellent approximation in typical capillary electrophoresis.

Eq. (17) indicates $p = p(z)$ only. However, $\mathrm{d}p/\mathrm{d}z$ in Eq. (16) is not necessarily a constant, say 0 for a purely electroosmotic

flow, representing the variation of temperature induced pressure gradients along the capillary. Thus, the right hand side term of Eq. (16) is independent of r. Integrating Eq. (16) twice with respect to r gives

$$u_z(r,z) = u_{eo}(z) - \frac{R_1^2}{4\mu(z)}\frac{dp}{dz}\left[1-\left(\frac{r}{R_1}\right)^2\right] \tag{23}$$

At this point, dp/dz remains unknown. We average each term in Eq. (23) over the capillary cross-section, and make some rearrangement to get:

$$\frac{dp}{dz} = [u_{eo}(z) - \bar{u}]\frac{8\mu(z)}{R_1^2} \tag{24}$$

Integrating Eq. (24) along the capillary length and noting $p(0) = p(L_0) = 0$ (i.e., no external pressure gradient is applied to the two ends of the capillary) yields:

$$\bar{u} = \int_0^{L_0}\mu(z)u_{eo}(z)dz \int_0^{L_0}\mu(z)dz \tag{25}$$

So, dp/dz is now accessible from Eq. (24), and varies along the capillary due to Joule heating and thermal end effects. Further from Eq. (23) we obtain the final formula for the axial fluid velocity

$$u_z(r,z) = u_{eo}(z) - 2[u_{eo}(z) - \bar{u}][1-(r/R_1)^2] \tag{26}$$

One can see that Eq. (26) is consistent with Ghosal's general formula to the leading order for electroosmotic flow in a microchannel of slowly varying cross-section and wall charge, where the lubrication approximation has been employed [39]. Therefore, Joule heating and thermal end effects not only alter the local electroosmotic velocity (the first term on the right hand side of Eq. (26)), but also induce axial-position dependent pressure-driven flows (the second term on the right hand side of Eq. (26)) in capillary electrophoresis. It is natural that the velocity entrance length is dependent on the thermal entrance length. The radial velocity component u_r can be obtained by substituting Eq. (26) into Eq. (18) and integrating over r once

$$u_r(r,z) = \frac{1}{2}\frac{du_{eo}}{dz}\left(\frac{r}{R_1}\right)\left[1-\left(\frac{r}{R_1}\right)^2\right] \tag{27}$$

Now, let us specify $\bar{u}$ in Eq. (26) by considering the temperature dependence of fluid properties. The calculation of du_{eo}/dz in Eq. (27) is straightforward and omitted here for compactness. As dilute aqueous solutions are often used in capillary electrophoresis, we assume their properties are identical to water. Most of these properties are temperature dependent and thus position dependent, here. Noting the definition of the slip velocity u_{eo} in Eq. (22), we can rewrite Eq. (25) as:

$$\bar{u} = \frac{-\varepsilon\zeta\int_0^L E(Z)dZ}{\int_0^L \mu(Z)dZ} \tag{28}$$

While numerical methods (e.g., Gaussian quadrature) can be employed to calculate the integrations in Eq. (28) for fluid properties of any forms of temperature dependence, we consider only the temperature dependence of viscosity in this paper. Both the dielectric constant and the zeta potential are assumed constant so as to obtain a relatively simple formula for the mean fluid velocity $\bar{u}$. The formula of fluid viscosity with respect to temperature is given by [9]:

$$\mu(T) = A\exp\left(\frac{B}{T}\right) \tag{29}$$

where $A = 2.761\times10^{-6}\,\mathrm{K\,gm^{-1}\,s^{-1}}$ and $B = 1713\,\mathrm{K}$. Expanding the exponential term in Eq. (29) as a Taylor series around $T = T_0$ and retaining only the first two orders yield:

$$\mu(Z) = \mu_0[1-\gamma\Theta(Z)] \tag{30a}$$

$$\gamma = \frac{B\Delta T}{T_0^2} \tag{30b}$$

where μ_0 indicates the viscosity at the room temperature. Similar to the approximation made in Eq. (9), Eq. (30a) and (30b) is only valid for small rises of fluid temperature. Substituting Eqs. (11a–d), (12) and (30a) and (30b) into Eq. (28) and in turn integrating it gives:

$$\bar{u} = \left\{1 - \frac{\gamma}{\beta^2}\left[1-\frac{1}{L}\frac{(e^{A_1L}-1)(e^{A_2L}-1)(1/A_1+1/A_2)}{e^{(A_2+A_2)L}-1}\right]\right\}^{-1} \times\left[-\frac{\varepsilon\zeta E_0}{\mu_0}\right] \tag{31a}$$

$$\bar{u} \cong \frac{1}{1-\gamma/\beta^2}\left[-\frac{\varepsilon\zeta E_0}{\mu_0}\right] \tag{31b}$$

where $L \gg 1$ and $e^{A_1L} = O(e^{A_2L}) \gg 1$ are indispensable to attain the simplified formula in Eq. (31b). The square bracketed term on the right end of Eqs. (31a) and (31b) is the electroosmotic velocity without Joule heating effects, whose prefactor, always larger than 1, reflects the flow enhancement effect of the fluid temperature rise. Moreover, the capillary length has hardly any influence on the flow rate unless the capillary is short (i.e., thermal end effects become pronounced), which is the intrinsic advantage of electroosmotic flow. The induced pressure distribution $p(z)$ along the capillary can be integrated from Eq. (24), and is omitted here.

2.4. Concentration field

The conservation of any chemical species, c, obeys the advection-diffusion equation

$$\frac{\partial c}{\partial t} + (\mathbf{u} + U_{ep})\cdot\nabla c = \nabla\cdot(D\nabla c) \tag{32}$$

where **u** is the fluid velocity vector, U_{ep} the electrophoretic velocity vector of a chemical species, and D the molecular diffusivity. Stokes–Einstein equation $D = k_B T/6\pi\mu a$ is often used to calculate the diffusion coefficient, where k_B is the Boltzmann's constant and a the radius of ionic species. The electrophoretic velocity may be estimated from Nernst–Einstein equation $U_{ep} = Dz_v eE/k_B T$, where z_v is the valence of ions and e the charge of a proton. Then, we find

$$U_{ep} = \frac{z_v eE}{6\pi\mu a} \tag{33}$$

Therefore, the sample transport is coupled with temperature and velocity fields. This coupling makes it difficult, if not impossible, to solve for c in Eq. (32) analytically. We will demonstrate in the next section that both thermal and velocity entrance lengths are much smaller than the capillary length. Moreover, the initial sample plug is generally a distance away from the capillary inlet in capillary electrophoresis. Therefore, the entrance region has negligible influence on the transport of samples.

In the fully developed region, the non-dimensional fluid temperature is $1/\beta^2$ as provided above, the slip velocity U_{eo} in Eq. (22) and the electrophoretic velocity U_{ep} in Eq. (33) are respectively specified as:

$$U_{eo} = -\frac{J\varepsilon\zeta}{\mu_0\lambda_0}\frac{1-\alpha\Delta T/\beta^2}{1-\gamma/\beta^2} \tag{34}$$

$$U_{ep} = \frac{Jz_v e}{6\pi\mu_0 a\lambda_0}\frac{1-\alpha\Delta T/\beta^2}{1-\gamma/\beta^2} \tag{35}$$

Noting $J(1-\alpha\Delta T/\beta^2)/\lambda_0 \geq \phi_0 R_l/L = E_0$ from Eq. (14a), both U_{eo} and U_{ep} are enhanced by Joule heating effects. In a coordinate system whose origin moves at the mean migration velocity of the chemical species $u_m = \bar{u} + U_{ep}$, Eq. (32) can be rewritten as:

$$\frac{\partial c}{\partial t} + (\bar{u} - U_{eo})\left[1 - 2\left(\frac{r}{R_l}\right)^2\right]\frac{\partial c}{\partial z_1} = D_m\frac{\partial^2 c}{\partial z_1^2} + D_m\frac{1}{r}\frac{\partial}{\partial r}\left(r\frac{\partial c}{\partial r}\right) \tag{36}$$

where D_m denotes the diffusivity in the fully developed region and $z_1 = z - u_m t$. Taylor first used Eq. (36) to study the dispersion of solute through a tube due to a combined effect of diffusion and convection [13]. Since then numerous related papers have appeared in the literature [14,40,41]. It is demonstrated that the mean concentration over the capillary cross-section, $\bar{c}$, to a first approximation, is governed by an equation of the form:

$$\frac{\partial \bar{c}}{\partial t} = K\frac{\partial^2 \bar{c}}{\partial z_1^2} \tag{37a}$$

$$K = D_m + \frac{(\bar{u} - U_{eo})^2 R_l^2}{48 D_m} \tag{37b}$$

where K indicates the well-known dispersion coefficient which is equivalent to but typically higher than the diffusion coefficient in molecular diffusion. In the absence of Joule heating effects, K is reduced to D_0 denoting the diffusivity at the room temperature. Joule heating affects the dispersion of samples via the enhancement of molecular diffusion and the induced pressure-driven flow of fluid. In practice, the perturbed electrophoretic velocity profile caused by radial temperature gradients contributes to the sample dispersion as well [30].

Here, we consider two types of transport processes of samples that often take place in microfluidic devices. In the first case, the capillary is initially filled with the solvent only, and the sample of uniform concentration c_0 is allowed to enter the capillary at time $t = 0$ (i.e., $\bar{c}(t, 0) = c_0$). Then, the solution to Eqs. (37a) and (37b) is:

$$\bar{c} = c_0 \mathrm{erfc}\left(\frac{z - u_m t}{2\sqrt{Kt}}\right) \tag{38}$$

where erfc(x) denotes the complementary error function, and the axial coordinate z has been recovered from $z_1 = z - u_m t$. The intrinsic feature of the complementary error function shows that the sample front advances with the mean migration velocity u_m, and diffuses to the downstream with a diffusion coefficient K. Behind the front, the sample concentration is uniformly c_0 and the dispersion due to molecular diffusion disappears. In the second case, a sample plug of uniform concentration c_0 and width $2w_0$ is initially injected to the capillary inlet (i.e., $\bar{c}(0, z) = c_0$ at $0 \leq z \leq 2w_0$). For this case, the solution to Eqs. (37a) and (37b) is given by:

$$\bar{c} = \frac{c_0}{2}\left[\mathrm{erf}\left(\frac{2w_0 - z + u_m t}{2\sqrt{Kt}}\right) + \mathrm{erf}\left(\frac{z - u_m t}{2\sqrt{Kt}}\right)\right] \tag{39}$$

where erf(x) denotes the error function. The summation of two error functions in Eq. (39) ensures that the sample is kept in a zone when it moves with the velocity u_m. Everywhere outside this zone, however, the sample concentration is zero. This feature gives rise to the method of electrophoretic separations. In addition, the sample zone is expanded to both downstream and upstream directions as if it diffuses with a diffusion coefficient K. In this paper, we will focus on the second case. The effects of Joule heating on the sample zone transport are analyzed below.

It is clear from previous analysis that Joule heating effects enhance both the mean fluid velocity $\bar{u}$ in Eqs. (31a) and (31b) and the electrophoretic velocity U_{ep} in Eq. (35), so does the mean migration velocity u_m of the chemical species. Therefore, the sample zone will take less time to arrive at the detector that is fixed at a distance away from the capillary outlet. In other words, Joule heating effects reduce the analysis time of capillary electrophoresis. However, Joule heating effects also contribute to the sample dispersion that is dependent on $\sqrt{Kt}$ in Eq. (39). If the elution time, t_m, for the sample to migrate from the inlet to the detector is taken into

consideration, we find

$$\sqrt{Kt_m} = \sqrt{\left[\frac{D_m}{u_m} + \frac{(\bar{u} - U_{eo})^2 R_l^2}{48 D_m u_m}\right] L_{det}} \quad (40)$$

where L_{det} is the distance from the capillary inlet to the detector. Clearly, the first term in the square bracket represents the dispersion due to the increased molecular diffusion, while the second one gives the dispersion due to the pressure-driven flow caused by thermal end effects. As demonstrated in Appendix B, the increase in molecular diffusion is partly balanced by the increase in migration velocity. Consequently, the real increase in the sample dispersion is reflected solely by the increase of fluid temperature. The magnitude of $\bar{u} - U_{eo}$ in Eq. (40) is very sensitive to the capillary length, and could be negligible if the capillary is sufficiently long where thermal ends effects are essentially small (see also Appendix B). For short capillaries like those microfabricated in lab-on-a-chip devices, however, the sample dispersion due to the induced pressure-driven flow has to be considered.

3. Results and discussion

In this section, we examine quantitatively the Joule heating and thermal end effects on capillary electrophoresis. The resultant alterations in the steady state temperature field, applied electric potential field, flow field, and the transient concentration field are demonstrated with the analytical formulae derived above. Unless otherwise indicated, fluid properties and working parameters used in the calculations are: thermal conductivities, $k_l = 0.6\,W\,m^{-1}\,K^{-1}$, $k_w = 1.5\,W\,m^{-1}\,K^{-1}$ and $k_p = 0.15\,W\,m^{-1}\,K^{-1}$; electrical conductivity, $\lambda_0 = 0.15\,S\,m^{-1}$ and $\alpha = 0.02\,K^{-1}$; dielectric constant, $\varepsilon = 80 \times 8.854 \times 10^{-12}\,CV^{-1}\,m^{-1}$; radii, $R_l = 50\,\mu m$, $R_w = 160\,\mu m$ and $R_p = 180\,\mu m$; Zeta potential, $\zeta = -30\,mV$; surface heat transfer coefficient, $h = 130\,W\,m^{-2}\,K^{-1}$ [9,18,19,22]. Note that the electrophoretic velocity is calculated from Eq. (35) without the need of using the electrophoretic mobility. We first calculated the electric current density from Eq. (15). The mean fluid velocity was then found from Eqs. (31a) and (31b). After that, the fluid temperature in Eq. (11a–d) was obtained. The axial fluid velocity in Eq. (26) and the radial fluid velocity in Eq. (27) were therefore available. Finally, the sample concentration was predicted from either Eqs. (39) or (40). More accurate values of the electric current density and the mean fluid velocity can be solved simultaneously from the coupled Eqs. (14a), (14b), (31a) and (31b), which are necessary on the circumstances of short capillaries. These values were used to predict the axial pressure distribution from Eq. (24).

Fig. 1 shows the electric current through the buffer solution at different electric fields. In the absence of Joule heating effects, the electric current $\lambda_0 E_0 \pi R_l^2$ is simply a linear function of the applied electric field. On considering the Joule heating effects, Eq. (15) predicts a higher electric current $J\pi R_l^2$ at every electric field. Moreover, the higher the electric field, the larger are the elevations in the fluid temperature and the electric current. This phenomenon has been observed previously [24,27,42]. Note that the increase of electric current (actually the electrical conductivity) has been a method to estimate the rise of fluid temperature for a long time [18,19,43].

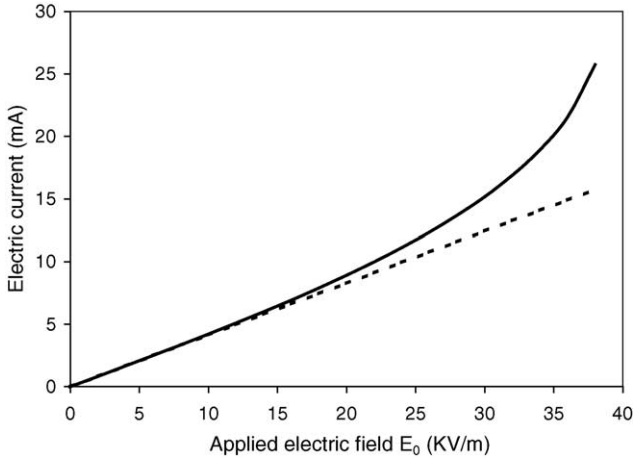

Fig. 1. Comparison of the electric current through the buffer solution with (solid line) and without (dashed line) considering Joule heating effects, respectively.

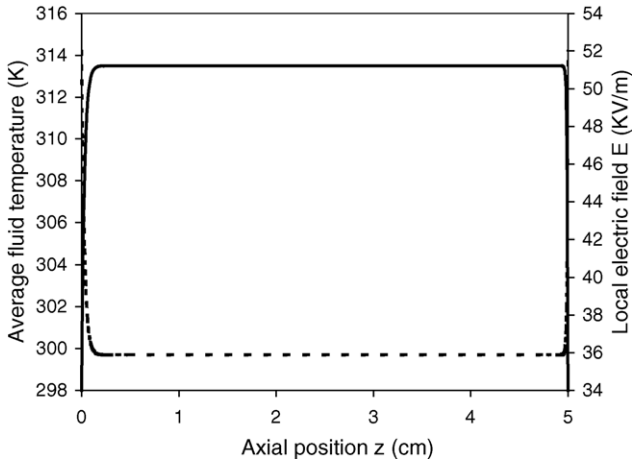

Fig. 2. Axial distributions of the average fluid temperature (solid line) and the local electric field (dashed line). The externally applied electric field is $E_0 = 36\,KV/m$. A 5 cm long capillary is chosen for an illustration.

Fig. 2 shows the axial distribution of the average fluid temperature at an applied electric field $E_0 = 36\,KV/m$ in a 5 cm long capillary. Note that the typical capillary length in capillary electrophoresis is tens of centimeters. For the capillary-based electrophoresis that takes place in a lab-on-a-chip device, however, the channel is usually several centimeters in length. We have pointed out earlier that the fluid temperature in the fully developed region is independent of the capillary length if this length is much larger than the capillary internal diameter. As the capillary is shortened, reservoir-based thermal end effects become pronounced. The fluid temperature in the main part of the capillary will thus be

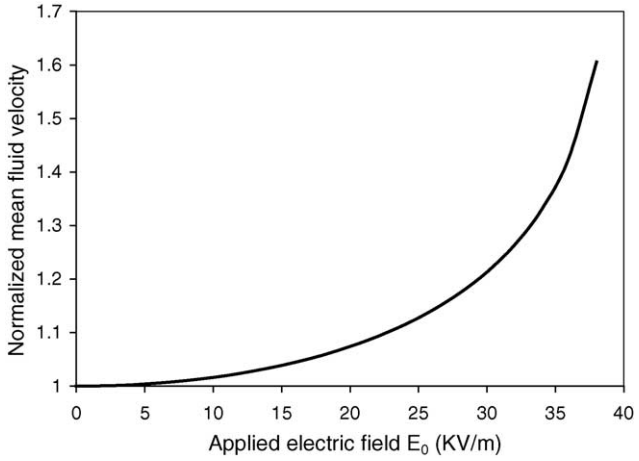

Fig. 3. Mean fluid velocity at different applied electric fields E_0. This velocity has been normalized by the value without considering Joule heating effects. The curve shows the enhancement of fluid velocity due to Joule heating effects. All working parameters are identical to those in Fig. 2.

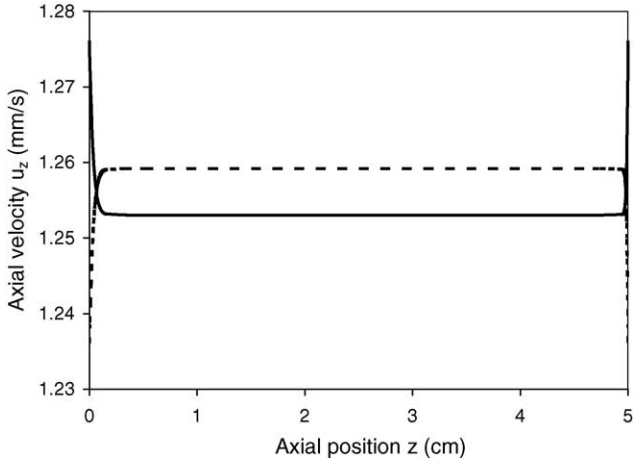

Fig. 4. Longitudinal distributions of the axial fluid velocity at the capillary wall (solid line) and along the capillary axis (dashed line), respectively. All working parameters are identical to those in Fig. 2.

decreased. Identical with our previous numerical and experimental studies [21,24], the axial temperature profile is not symmetrical, inclined to the downstream due to the advective effect of fluid flow. Sharp temperature drops are predicted close to the capillary ends while a high temperature plateau exists in the middle section. While the thermal entrance length is of approximately 20 times of the capillary internal radius, the thermal exit length is of only about five times of the capillary internal radius. Fig. 2 also displays the axial distribution of the local electric field E. In order to meet the current continuity, the electric fields close to capillary ends have to be significantly higher than the nominal electric fiend E_0 applied externally. In the middle section of the capillary, however, the local electric field is a little bit lower than E_0 as the total voltage drop over the whole capillary is fixed [30].

Fig. 3 shows the enhancement of mean fluid velocity (i.e., the flow rate per unit cross-sectional area) in a 5 cm-long capillary due to Joule heating and thermal end effects. This velocity has been normalized by the value without considering Joule heating effects. Therefore, the normalized fluid velocity corresponds exactly to the prefactor of the right hand side term in Eqs. (31a) and (31b). Similar to the trend of electric current with respect to the applied electric field E_0, the mean fluid velocity is increased more significantly at higher electric fields [24,27,42]. Therefore, Joule heating induced fluid temperature increase can enhance the throughput and reduce the separation time of capillary electrophoresis. For example, at $E_0 = 36$ KV/m, the average fluid temperature in the main part of the capillary is increased by only 5% (from 298 to 313.5 K, see Fig. 2). However, the mean fluid velocity is increased by more than 40%.

Fig. 4 shows the longitudinal distribution of axial fluid velocity u_z in a capillary. Both the velocity along the capillary axis and the one at the capillary wall (i.e., the slip velocity in Eq. (22)) are demonstrated. In regions close to capillary ends, the rise of local electric field (see the dashed line in Fig. 2) is partly counterbalanced by the higher fluid viscosity due to the temperature drop (see the solid line in Fig. 2). As a result, the slip velocity is higher close to the capillary ends, where the axial fluid velocity along the capillary centerline is lower than the rest. In other words, axial pressure gradients are brought about to meet the requirement of mass continuity. The sine-shaped pressure distribution along the capillary is displayed in Fig. 5. Positive pressure gradients appear close to the capillary ends making the local fluid velocity profile concave over the cross-section. A negative pressure gradient exists in the middle section of the capillary so that the velocity profile is slightly convex, which has been experimentally observed [24,44]. Fig. 6 demonstrates different radial profiles of the axial fluid velocity at different positions along the capillary. The convex curvature in the middle section is much smaller than the concave curvature close to capillary ends.

Fig. 7 shows the distribution of sample concentration averaged over the cross-section, $\overline{c}$, when the sample zone

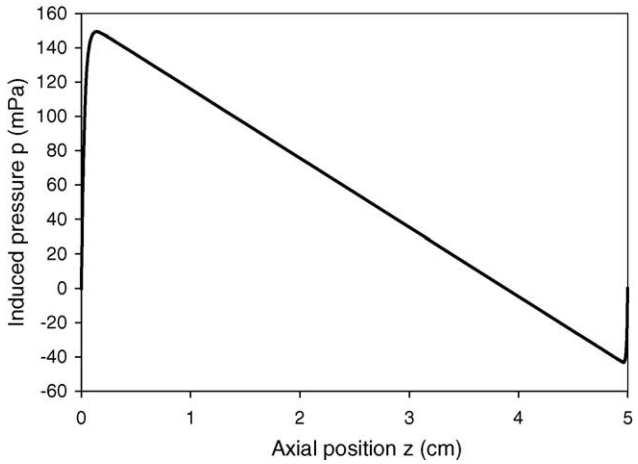

Fig. 5. Axial distribution of the pressure induced by Joule heating and thermal end effects in capillary electrophoresis. All working parameters are identical to those in Fig. 2.

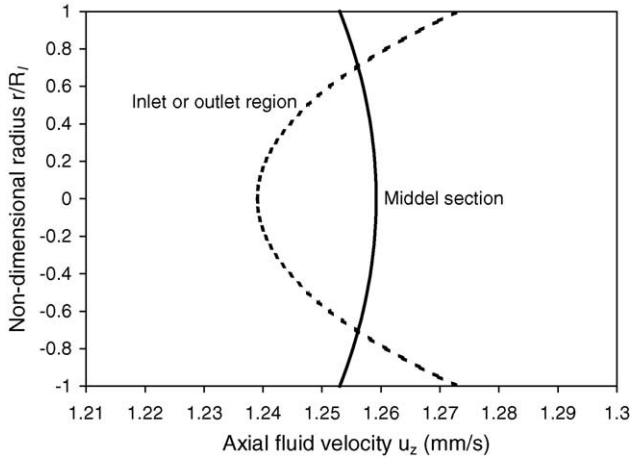

Fig. 6. Radial profiles of the axial fluid velocity at two different positions of the capillary. The dashed line shows the profile one internal radius away from the capillary inlet. The solid line gives the profile in the middle of the capillary length. All working parameters are identical to those in Fig. 2.

migrates through the capillary. As the total mass of the sample is conserved during the transportation, the area underneath every "pulse" remains invariant. Consequently, the sample zone becomes wider if its peak concentration is lowered, meaning that the sample is dispersed. One can see that Joule heating effects make the sample zone move faster. Also, the sample dispersion is more significant after the same elution time, which can be identified from the decrease of the peak concentration (solid lines) compared to that without Joule heating effects (dashed lines). Whereas the increase of migration velocity of a sample could reduce the separation time in capillary electrophoresis, the larger sample dispersion might decrease the separation efficiency. In order to figure out this, Fig. 8 compares the mean concentration and the elution time

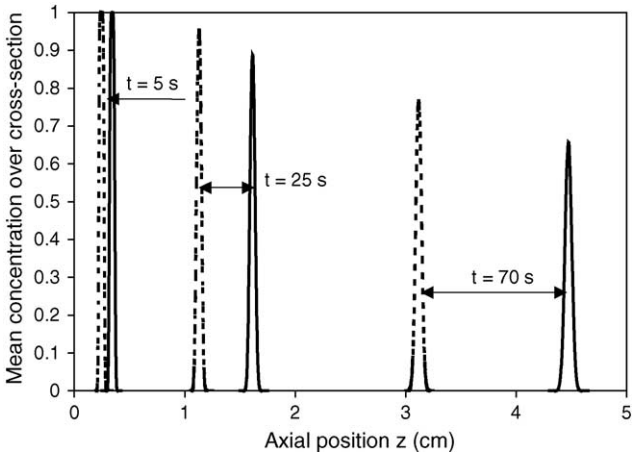

Fig. 7. Mean concentration of a sample over the cross-section at different times. The solid lines indicate the distributions along the capillary with the consideration of Joule heating effects. The dashed lines are the distributions without Joule heating effects. The charge and radius of ions is $z_v = -1$ and $a = 0.8$ nm, respectively. The width of the initial sample plug is 5 internal radii ($2w_0 = 5R_l$), and its concentration is $c_0 = 1$. All other working parameters are identical to those in Fig. 2.

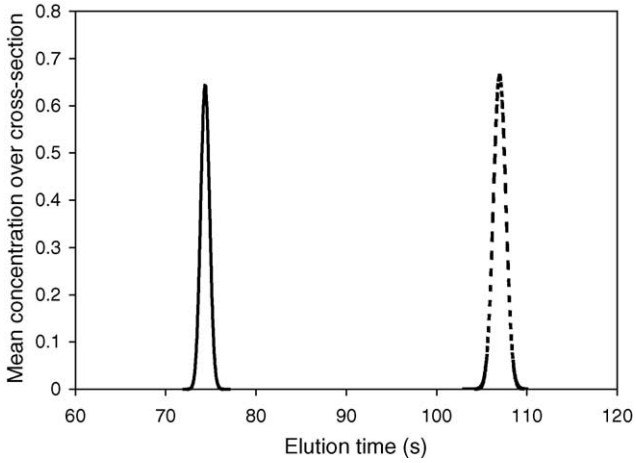

Fig. 8. Mean concentration over the cross-section with respect to the elution time when the sample zone passes by the detector. The solid line denotes the sample transport with the consideration of Joule heating effects. The dashed line corresponds to the case without Joule heating effects. The detector is 0.5 cm away from the capillary outlet. All other working parameters are identical to those in Fig. 7.

of the sample when it passes by a detector fixed at a distance away from the capillary outlet. On account of Joule heating effects, it takes much less time to transport the sample to the detector. Also, the sample zone passes by the detector more quickly than that without Joule heating effects. However, we notice that the peak concentration at the detector is slightly lower (i.e., the sample zone is wider, and thus has larger dispersion) when Joule heating effects are considered.

Fig. 9 shows the comparison of the theoretical (solid curve) and the experimental (symbols) concentration profiles

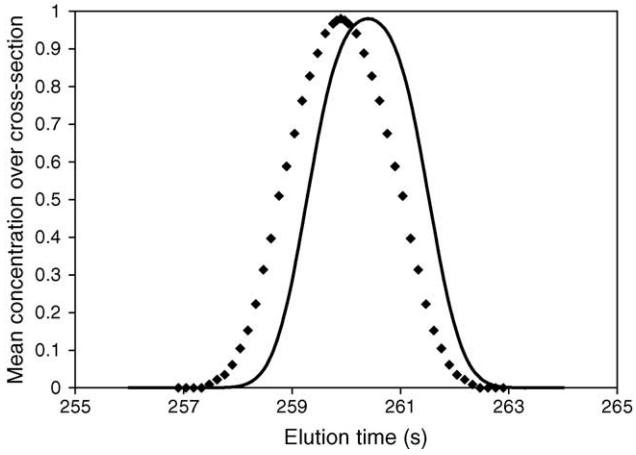

Fig. 9. Comparison of theoretical (solid curve) concentration profile of sample passing by the detector with that observed in Delinger and Davis's experiments [45]. The peak height of the experimental profile is assumed the same as that of the theoretical profile while the height of the base line is set zero. Working parameters different from those given in the text include: $E_0 = 25$ KV/m, $L_0 = 60$ cm, $L_{det} = 51$ cm, $R_l = 37.5$ μm, $R_w = 167.5$ μm, $R_p = 187.5$ μm, the width of the initial sample plug $2w_0 = 4.4$ mm, EO mobility 5.28×10^{-8} m^2 V^{-1} s^{-1} at 22 °C, electrical conductivity $\lambda_0 = 0.263$ S m^{-1} at 22 °C, and molecular diffusivity $D_0 = 1.25 \times 10^{-9}$ m^2 s^{-1} at 22 °C [45].

when the sample (acetone as the marker of electroosmotic flow [45]) passes the detector. The experimental data were taken from Delinger and Davis's measurements (middle left subfigure in Fig. 7 of ref. [45]). As these authors did not provide the scale of their concentration data, we assumed that the peak height of the experimental profile coincides with that of the theoretical profile while the height of the base line is set to be zero. From Fig. 9 one can see that both the shape of concentration profile and the elution time predicted from the proposed model in this paper are in close agreement with the experimentally measured profile. Therefore, the present model provides accurate evaluation of the Joule heating effects on electrokinetic transportation in capillary electrophoresis.

4. Conclusions

In ideal capillary electrophoresis, the profiles of fluid electroosmotic flow and species electrophoretic flow are both plug-like. Molecular diffusion is the only source of sample zone broadening. In practice, however, many factors can affect the above flow patterns, of which Joule heating is one that always exists. We have developed an analytical model to study Joule heating and thermal end effects in capillary electrophoresis. By de-coupling the energy equation and the momentum equation, close-form formulae have been derived for the steady state temperature field, applied electric potential field, pressure field, velocity field and the transient concentration field. We have also obtained compact analytical formulae for the electric current and the mean fluid velocity (i.e., the volume flow rate per unit cross-sectional area). These formulae could provide a clear understanding of Joule heating and thermal end effects on the transport of heat, electricity, momentum and mass species in capillary electrophoresis.

With the analytical formulae presented in this paper, we have demonstrated graphically that, due to the thermal end effects, sharp temperature drops exist close to capillary ends, where electric fields rise significantly. Axial-position dependent pressure gradients have to be induced to realize the mass continuity. As a result, concave–convex–concave fluid velocity profiles appear from the inlet to the outlet of the capillary. These predictions are consistent with our previous numerical simulation and have already been verified experimentally. In addition, Joule heating effects enhance the transport of samples, which could reduce the analysis time in capillary electrophoretic separations. However, Joule heating and thermal end effects also increase the sample dispersion, and thus decrease the separation efficiency.

Acknowledgement

Financial support from the Natural Sciences and Engineering Research Council (NSERC) of Canada, through a research grant to D. Li is gratefully acknowledged.

Appendix A

According to its definition, the non-dimensional thermal entrance length δ is solved from

$$0.99\frac{1}{\beta^2} = \frac{1}{\beta^2}\left[1-\frac{(e^{A_1 L}-1)e^{A_2(L-Z)}+(e^{A_2 L}-1)e^{A_1 Z}}{e^{(A_2+A_2)L}-1}\right] \tag{A.1}$$

Rearrange Eq. (A.1),

$$0.99=1-\frac{e^{-A_2\delta}-e^{-A_1 L-A_2\delta}+e^{A_1(\delta-L)}+e^{A_1\delta-(A_1+A_2)L}}{1-e^{-(A_1+A_2)L}} \tag{A.2}$$

Noting $L \gg \delta$ and $L \gg 1$, we neglect all exponential terms involving the power of $-L$. Then, the last equation is reduced to

$$e^{-A_2\delta} = 0.01 \tag{A.3}$$

It is now straightforward to get

$$\delta = \ln 100/A_2 \tag{A.4}$$

Recovering the dimensional form and evaluating the natural logarithm finally gives rise to the thermal entrance length provided in the text.

Appendix B

Noting the non-dimensional fluid temperature in the fully developed region is $1/\beta^2$, the diffusion coefficient in this region is calculated as:

$$D_m = D_0\frac{1+\Delta T/T_0\beta^2}{1-\gamma/\beta^2} \tag{B.1}$$

where $D_0 = k_B T_0/6\pi\mu_0 a$ indicates the diffusivity at the room temperature. The summation of Eqs. (31b) and (35) leads to the mean migration velocity of chemical species

$$u_m = u_0\frac{1}{1-\gamma/\beta^2} \tag{B.2}$$

$$u_0 = -\frac{\varepsilon\zeta E_0}{\mu_0}+\frac{z_v e E_0}{6\pi\mu_0 a} \tag{B.3}$$

where u_0 is exactly the migration velocity in the absence of Joule heating effects, and Eq. (14b) has been invoked in the manipulation since $L \gg 1$ in typical capillary electrophoresis. For short capillaries like those fabricated in a microchip, however, full formulae for both the temperature field in Eq. (11a) and the electric field in Eq. (14a) have to be used. The dispersion due to molecular diffusion in Eq. (40) is now spec-

ified as:

$$\sqrt{\frac{D_m}{u_m}L_{det}} = \sqrt{\frac{D_0}{u_0}L_{det}(1+\Delta T/T_0\beta^2)} \quad \text{(B.4)}$$

Therefore, Joule heating effects increase the diffusion induced sample dispersion via only the rise of fluid temperature. Also from Eq. (14b) when $L \gg 1$, the slip velocity in Eq. (34) through a long capillary is reduced to

$$U_{eo} = -\frac{\varepsilon\zeta E_0}{\mu_0}\frac{1}{1-\gamma/\beta^2} \quad \text{(B.5)}$$

which is identical to the mean fluid velocity $\bar{u}$ in Eqs. (31a) and (31b). As a result, the dispersion due to the induced pressure-driven flow in Eq. (40) is negligible if the performed capillary is sufficiently long.

References

[1] D.J. Harrison, K. Fluri, K. Seiler, Z. Fan, C.S. Effenhauser, A. Manz, Science 261 (1993) 895.
[2] H.A. Stone, A.D. Stroock, A. Ajdari, Annu. Rev. Fluid Mech. 36 (2004) 381.
[3] J.P. Landers, Handbook of Capillary Electrophoresis, second ed., CRC Press, Boca Raton, FL, 1997.
[4] B. Gas, M. Stedry, E. Kenndler, Electrophoresis 18 (1997) 2123.
[5] B. Gas, E. Kenndler, Electrophoresis 21 (2000) 3888.
[6] B. Gas, E. Kenndler, Electrophoresis 23 (2002) 3817.
[7] J.H. Knox, I.H. Grant, Chromatographia 24 (1987) 135.
[8] A.E. Jones, E. Grushka, J. Chromatogr. 466 (1989) 219.
[9] J.H. Knox, K.A. McCormack, Chromatographia 38 (1994) 207.
[10] E. Grushka, R.M. McCormick, J.J. Kirkland, Anal. Chem. 61 (1989) 241.
[11] S. Bello, P.G. Righetti, J. Chromatogr. 606 (1992) 95, 103.
[12] S. Ghosal, Electrophoresis 25 (2004) 214.
[13] G. Taylor, Proc. R. Soc. Lond. A 219 (1953) 186.
[14] R. Aris, Proc. R. Soc. Lond. A 235 (1956) 67.
[15] K. Swinney, D.J. Bornhop, Electrophoresis 23 (2002) 613.
[16] K.K. Liu, K.L. Davis, M.D. Morris, Anal. Chem. 66 (1994) 3744.
[17] D. Ross, M. Gaitan, L.E. Locascio, Anal. Chem. 73 (2001) 4117.
[18] S. Palonen, M. Jussila, S.P. Porras, T. Hyotylainen, M. Riekkola, J. Chromatogr. A 916 (2001) 89.
[19] S.P. Porras, E. Marziali, B. Gas, E. Kenndler, Electrophoresis 24 (2003) 1553.
[20] A.S. Rathore, J. Chromatogr. A 1037 (2004) 431.
[21] X. Xuan, D. Li, J. Micromech. Microeng. 14 (2004) 1171, and references cited therein.
[22] H.J. Peterson, R.P. Nikolajsen, K.B. Mogensen, J.P. Kutter, Electrophoresis 25 (2004) 253.
[23] X. Xuan, D. Sinton, D. Li, Int. J. Heat Mass Trans. 47 (2004) 3145, and references cited therein.
[24] X. Xuan, B. Xu, D. Sinton, D. Li, Lab. Chip 4 (2004) 230, and references cited therein.
[25] G.Y. Tang, C. Yang, C.J. Chai, H.Q. Gong, Langmuir 19 (2004) 10975.
[26] G.Y. Tang, C. Yang, C.K. Chai, H.Q. Gong, Anal. Chim. Acta 507 (2004) 27.
[27] D. Sinton, X. Xuan, D. Li, Exp. Fluid 37 (2004) 872.
[28] B. Gas, J. Chromatogr. 644 (1993) 161.
[29] R. Chien, J.C. Helmer, Anal. Chem. 63 (1991) 1354.
[30] X. Xuan, D. Li, Electrophoresis 26 (2005) 166.
[31] A.E. Herr, J.I. Molho, J.G. Santiago, M.G. Mungal, T.W. Kenny, M.G. Garguilo, Anal. Chem. 72 (2000) 1053.
[32] S. Ghosal, Anal. Chem. 74 (2002) 4198.
[33] S. Ghosal, J. Fluid. Mech. 491 (2003) 285.
[34] J.L. Anderson, W.K. Idol, Chem. Eng. Commun. 38 (1985) 93.
[35] E.V. Dose, G. Guiochon, J. Chromatogr. A 652 (1993) 263.
[36] J.M. MacInner, Chem. Eng. Sci. 57 (2002) 4539.
[37] W.M. Deen, Analysis of Transport Phenomena, Oxford University Press, New York, 1998.
[38] R.J. Hunter, Zeta Potential in Colloid Science Principals and Applications, Academic Press, New York, 1981.
[39] S. Ghosal, J. Fluid. Mech. 459 (2002) 103.
[40] W.N. Gill, Proc. Roy. Soc. Lond. A 298 (1967) 335.
[41] W.N. Gill, R. Sankarasubramanian, Proc. Roy. Soc. Lond. A 316 (1970) 341.
[42] D. Erickson, D. Sinton, D. Li, Lab. Chip 3 (2003) 141.
[43] D.S. Burgi, K. Salomon, R. Chien, J. Liq. Chromatogr. 14 (1991) 847.
[44] T.J. Johnson, D. Ross, M. Gaitan, L.E. Locascio, Anal. Chem. 73 (2001) 3656.
[45] S.L. Delinger, J.M. Davis, Anal. Chem. 64 (1992) 1947.